Volume 26
Number 10
14 March 2024
Pages 7933–8560

PCCP

Physical Chemistry Chemical Physics

rsc.li/pccp

25 YEARS ANNIVERSARY

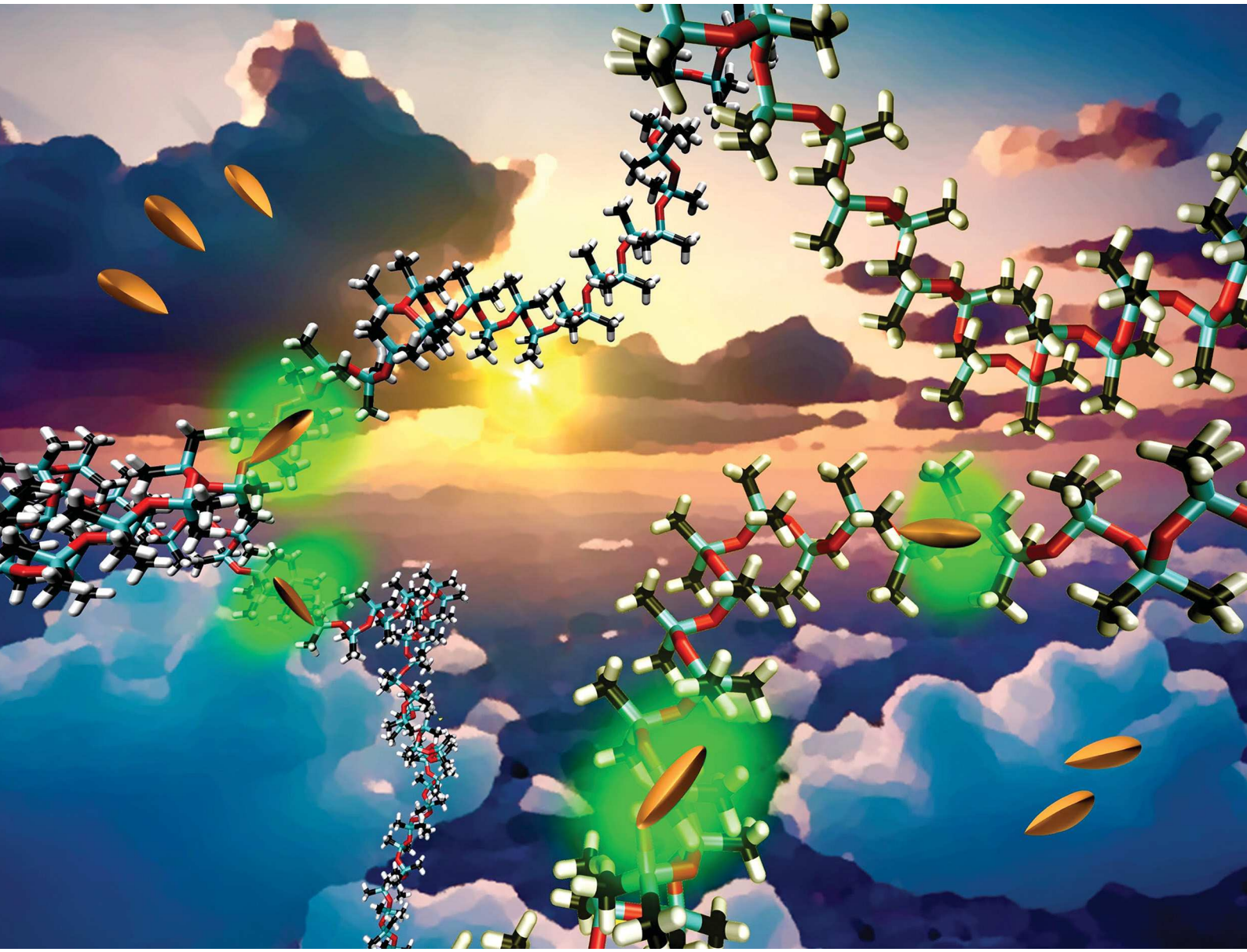

ISSN 1463-9076

ROYAL SOCIETY OF CHEMISTRY

PAPER

Valentine I. Vullev *et al.*

Poly(dimethylsiloxane) as a room-temperature solid solvent for photophysics and photochemistry

PCCP Owner Societies

PCCP

PAPER

View Article Online
View Journal | View Issue

Cite this: *Phys. Chem. Chem. Phys.*, 2024, **26**, 8062

Poly(dimethylsiloxane) as a room-temperature solid solvent for photophysics and photochemistry†

John A. Clark,[a] Samantha Robinson,[a] Eli M. Espinoza,[b] Duoduo Bao,[a] James B. Derr,[c] Luca Croft,[a] Omar O'Mari,[a] William H. Grover[a] and Valentine I. Vullev*[abcd]

Received 7th November 2023,
Accepted 5th February 2024

DOI: 10.1039/d3cp05413f

rsc.li/pccp

Medium viscosity strongly affects the dynamics of solvated species and can drastically alter the deactivation pathways of their excited states. This study demonstrates the utility of poly(dimethylsiloxane) (PDMS) as a room-temperature solid-state medium for optical spectroscopy. As a thermoset elastic polymer, PDMS is transparent in the near ultraviolet, visible, and near infrared spectral regions. It is easy to mould into any shape, forming surfaces with a pronounced smoothness. While PDMS is broadly used for the fabrication of microfluidic devices, it swells in organic solvents, presenting severe limitations for the utility of such devices for applications employing non-aqueous fluids. Nevertheless, this swelling is reversible, which proves immensely beneficial for loading samples into the PDMS solid matrix. Transferring molecular-rotor dyes (used for staining prokaryotic cells and amyloid proteins) from non-viscous solvents into PDMS induces orders-of-magnitude enhancement of their fluorescence quantum yield and excited-state lifetimes, providing mechanistic insights about their deactivation pathways. These findings demonstrate the unexplored potential of PDMS as a solid solvent for optical applications.

Introduction

This publication shows the utility of poly(dimethylsiloxane) (PDMS) as a solid solvent at room-temperature for exploring the excite-state dynamics of two molecular-rotor dyes, 3,3′-diethylthiacyanine (THIA) iodide and thioflavin T (ThT) (Chart 1), that are principally used as biological fluorescence stains.[1–8] The ease of preparing transparent blocks and slabs of PDMS, along with the mild conditions of loading dyes into them, makes this spectroscopy method (with unexplored potentials) attractive and highly promising.

Solid-state solvating matrices restrict conformational dynamics and translational degrees of freedom, permitting the emergence of excited-state pathways that are undetectable in liquid solutions. When large-amplitude structural relaxations drive dominating non-radiative decays in non-viscous solutions, for example, observing radiative and other parallel deactivation pathways requires rigid media. Employing solid optically transparent solvents has led to important discoveries, such as the first demonstration of the Marcus inverted region.[9–11]

Flash-frozen organic solutions, where the solvents form solid glass structures, offer the rigid environment required for phosphorescence and Stark-spectroscopy measurements, for example.[12–17] The rigidity of such frozen solvent media offers unique insights for charge-transfer and single-molecule analyses.[18,19] Besides the increased complexity of cryogenic setups, the liquid-nitrogen temperatures are irrelevant to biological systems and the ambient conditions of every-day life.

Introducing molecular samples into porous solids, such as zeolites, provides a rigid environment at elevated temperatures.[20–32] Questions about transparency, reliability of

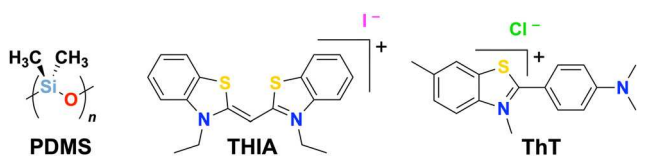

Chart 1 Structures of THIA and ThT, along with the generic structure of PDMS.

[a] Department of Bioengineering, University of California, Riverside, CA 92521, USA. E-mail: vullev@ucr.edu
[b] Department of Chemistry, University of California, Riverside, CA 92521, USA
[c] Department of Biochemistry, University of California, Riverside, CA 92521, USA
[d] Materials Science and Engineering Program, University of California, Riverside, CA 92521, USA

† Electronic supplementary information (ESI) available. See DOI: https://doi.org/10.1039/d3cp05413f

loading, and distribution homogeneity of the samples appear to linger over the utility of zeolites for optical applications.

Sucrose octaacetate (SOA) is a crystalline material that melts at about 87 °C. When allowed to cool under ambient conditions, molten SOA solidifies into transparent glass. Thus, dissolving molecular (or other) species in the molten SOA and letting it cool down results in room-temperature solid-state solutions.[33–40] Due to the formation of the SOA crystalline phase, however, such glass samples lose their transparency when kept for extended periods. Also, the elevated temperature of the molten SOA may compromise the stability of the examined species.

Dissolving molecular species in prepolymer mixtures, followed by polymerization, presents another approach for forming solid solutions.[41–45] Modifying the dyes with functional groups of the monomers allows them to covalently attach to the polymer chains during the polymerization and/or crosslinking processes.[46,47] Mixing chromophores with a prepolymer and a curing agent offers a means for doping PDMS with coloured and fluorogenic agents.[48–51] For the fidelity of such methods, however, the polymerization and curing crosslinking chemistry must not interfere with the doping species.

Adding dyes to molten thermoplastic polymers or their room-temperature solutions in volatile organic solvents and spin-coating or casting them result in solid films with chromophores incorporated in them.[47,52,53] The impossibility of melting thermoset polymers or dissolving them in organic solvents precludes the extension of this doping approach to them. Nevertheless, while PDMS is thermoset, it is a porous material.[54–57] When dye solutions flow through microfluidic chips made of PDMS, they tend to stain the polymer at the channel walls.[58] Reports by Oki *et al.* quantify such dye permeation in PDMS.[59,60] The depth of permeation depends on the solvent and the hydrophobicity of the dye.[61,62] Apart from such colour staining of PDMS components at micrometre and millimetre scales, the potentials of this post-curing doping of solid thermoset materials are still largely unexplored.

Despite its immense importance for fabricating microfluidic devices and other microelements with pronounced biocompatibility,[63–72] PDMS is not compatible with most organic solvents. A wide range of organic liquids swell PDMS, increasing its volume by a factor of two or more.[73] While this swelling in non-reactive solvents is reversible (*i.e.*, PDMS restores its shape and size upon removal of the solvent), it presents a principal limitation for the applicability of devices made of this polymer. Nevertheless, this disadvantage for microdevices can be immensely beneficial for loading PDMS with samples dissolved in the swelling solvents. Furthermore, PDMS is transparent between 280 and 1650 nm, making it promising for optical applications.[74,75] These considerations give confidence that PDMS can serve as a valuable solid solvating medium in molecular spectroscopy and photochemistry.

Herein, we examine the utility of PDMS as a solid-state solvent (Chart 1). Loading THIA and ThT into a PDMS matrix (Chart 1) decreases the rates of non-radiative decay of their electronically excited states by about three orders of magnitude, which pronouncedly increases their fluorescence quantum yields (ϕ_f). This PDMS-induced emission enhancement is comparable to that observed for THIA and ThT not only when placed in a solid SOA glass, but also when taken up by Gram-positive and Gram-negative bacterial cells.

Results and discussion

How to prepare the PDMS solid solvent?

Known as ''silicone rubber,'' PDMS is a broadly used material. It is easy to prepare and mould. Prepolymer PDMS chains mixed with a crosslinker, *i.e.*, a curing agent, form a viscous liquid that can be poured into a mould of non-silicone-based material that precludes strong adhesion.[76–79] Upon photo- or thermal curing, following degassing under vacuum, the mould features imprint on the PDMS surface with sub-micrometre resolution. This property of PDMS made it widely popular for fabricating microfluidic devices that strongly impacted biological, biomedical, and engineering research at the turn of this century.[80–94]

Employing inexpensive 1-cm polystyrene cuvettes with four polished sides as moulds allow us to prepare PDMS blocks that perfectly fit into the 1-cm sample holders of most spectrophotometers and spectrofluorometers. After pouring it into the polystyrene cuvettes and degassing it under vacuum, the prepolymer mixture (PDMS, SYLGARD™ 184) solidifies at room temperature in less than 24 hours (Fig. 1(a) and (b)). Breaking the polystyrene cuvette moulds and removing the broken pieces leave transparent blocks of PDMS with smooth walls (Fig. 1(c)).

While aliphatic amines and hydrocarbons are the best swelling solvents for PDMS,[73] they can prove reactive or provide insufficient solubility for many samples of interest. Conversely, suitable solvents such as DMSO and DMF do not swell PDMS.[73] Chlorinated solvents offer a compromise ensuring good swelling and sample solubility.[73] We select dichloromethane (DCM) which also has volatility needed for its expedient and facile removal from the swollen PDMS blocks.

Initial swelling in neat solvents (and replacing the solvent several times with fresh ones) allows the removal of the non-crosslinked polymer chains and other impurities remaining from the thermosetting process.[95] When swollen with organic solvents, PDMS may lose its transparency because of refractive-index mismatch (Fig. 1(d), left). Subjecting the DCM-swollen PDMS blocks to vacuum removes the solvent from them and restores their size, shape, and transparency (Fig. 1(d), right).

How to load samples in PDMS?

Placing the cleaned PDMS blocks (restored to their original sizes) in DCM solutions of THIA and ThT doubles their volume and loads the dyes into them (Fig. 1(e)). After soaking for 5 to 24 hours, we take the blocks out of the dye solutions, wash them with DCM and allow them to shrink to their original size by evaporating the solvent out of them (Fig. 1(f)–(h)).

The first and most important observation is that the PDMS blocks doped with THIA and ThT show strong fluorescence,

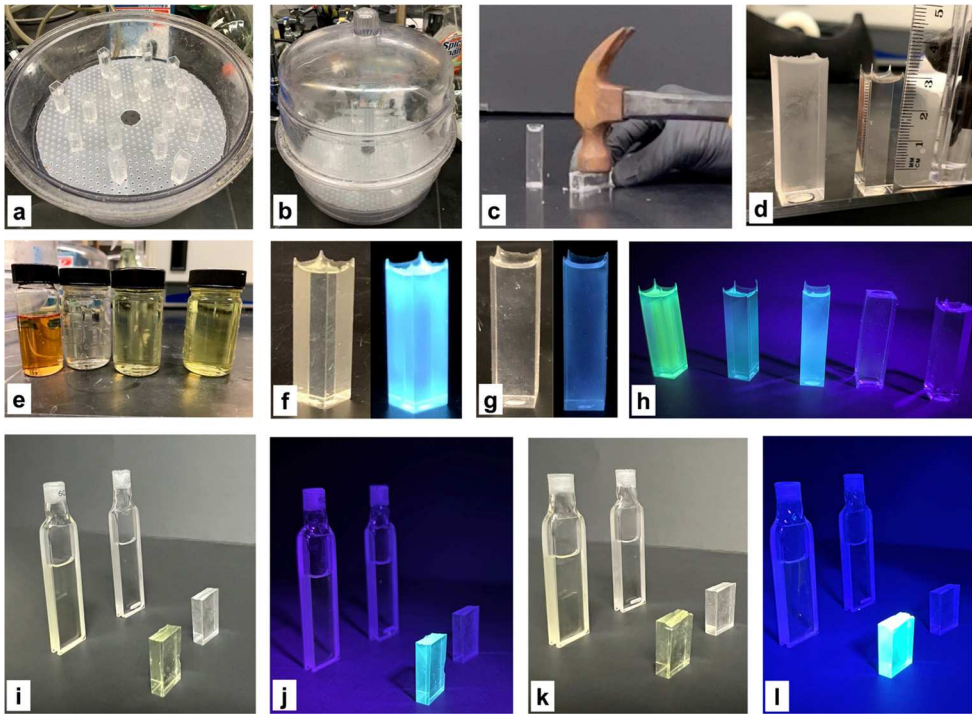

Fig. 1 Fabrication of PDMS blocks and loading them with dyes that are soluble in dichloromethane (DCM). (a) PDMS prepolymer mixture poured into polystyrene cuvettes with four polished sides that serve as molds. (b) Degassing the prepolymer mixture under vacuum and letting polymerize at room temperature. (c) Breaking a cuvette mold to extract the solidified PDMS block (see ESI† for a movie of this step of the procedure). (d) Images of (left) a PDMS block swollen with DCM and (right) a PDMS block reshrunk, after swelling and washing, by keeping it under vacuum to remove the DCM from it. (e) Swelling PDMS blocks in DCM solutions of various dyes. Vials are solutions with THIA ordered from left to right as 1 mM, 1 μM, 10 μM, and 100 μM. (f) and (g) Bright-field and fluorescence images of PDMS blocks loaded with (f) THIA and (g) ThT. (h) Fluorescence images of PDMS blocks soaked in DCM solutions of different dyes (from left to right: Ph-ANI, THIA, ThT, CR and blank with no dye added). After the soaking treatment, the blocks were washed and allowed to dry and shrink back to their original sizes. While Ph-ANI, THIA and ThT were absorbed by the polymer blocks, CR was not taken up. (i) and (k) Bright-field and (j) and (l) fluorescence images of (i) and (j) 10 μM THIA and (k) and (l) 20 μM ThT in DCM liquid solutions (in 2-mm quartz cuvettes) and loaded in 4-mm PDMS blocks. (i)–(l) For comparison, cuvettes with neat DCM and blank PDMS blocks with nothing loaded in them are placed on the back of the dye samples.

while DCM solutions of these dyes with the same concentrations do not (Fig. 1(i)–(l)). Furthermore, the intensity of the autofluorescence from the UV-illuminated PDMS blocks is negligibly small in comparison to the emission signals from the dyes (Fig. 1(j) and (l)).

A close examination of the PDMS blocks soaked in the THIA and ThT solutions reveals that in some cases their sides and edges fluoresce stronger than their bulk in the middle (Fig. 1(f)). Increasing the dye concentration in the DCM solution and shortening the soaking times enhances this heterogeneity of PDMS doping. Imaging cross-sections of the PDMS blocks clearly illustrates the extent of heterogeneity of the dye distribution (Fig. S5–S7, ESI†). The nature of the samples also affects their loading distribution. Using this DCM-soaking method for introducing non-charged dyes, such as *N*-phenyl-4-dimethylamino-1,8-naphthalimide (Ph-ANI),[96,97] yields improved homogeneity of the sample distribution in the PDMS blocks (Fig. 1(h), leftmost block). Conversely, ionic dyes with relatively poor solubility in chlorinated solvents, such as Congo red (CR), do not permeate the PDMS blocks even after extended soaking (Fig. 1(h)). As catanionic dyes, THIA and ThT are better than CR but they are not as good as Ph-ANI for loading them into PDMS by soaking in DCM solutions.

An inhomogeneous distribution of the chromophores within the polymer blocks can present challenges in quantifying results from right-angle emission measurements, for example. Resorting to thin PDMS blocks with a thickness of a few millimetres (Fig. 1(i)–(l)) allows such challenges to be addressed. While such narrow PDMS blocks warrant an increased dye loading to ensure sufficient optical density, they are useful for transmission-mode absorption and small-angle emission measurements utilizing face-on excitation.

The dye concentrations in the doped PDMS blocks are comparable or smaller than those in the swelling DCM solutions and depend on the duration of soaking (Fig. 2). When placed in the DCM dye solutions, the PDMS blocks swell relatively fast. While the solvent is taken up by the material within less than an hour, the data show that additional time is required for the PDMS to reach the desired dye concentration. It indicates that the solvent quickly permeates the bulk of the PDMS blocks and solvates the polymer chains. For the dye (dissolved in DCM) to load in the swollen blocks, it can take up to 24 hours or longer (Fig. 2).

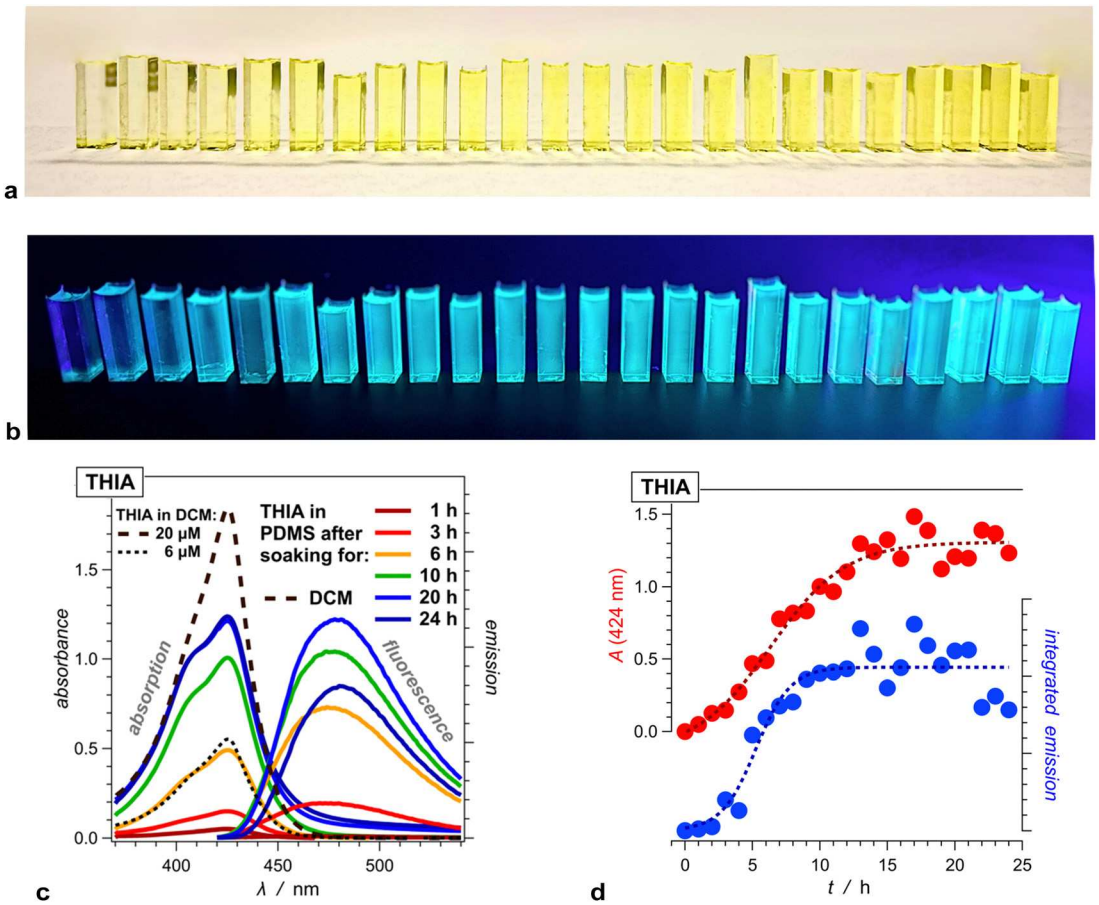

Fig. 2 Loading THIA in PDMS blocks by soaking them in 20 μM DCM solution of the dye for different durations of time. (a) Bright-field and (b) fluorescence images of the blocks soaked for 1 to 24 hours (λ_{ex} = 365 nm). The swelling and soaking of all 24 blocks in the same DCM THIA solution was initiated at the same time. Each hour, one block was taken out, washed with DCM, and allowed to shrink to its original size. (c) Absorption and emission spectra of THIA in the PDMS blocks soaked for different durations of time. For comparison, the absorption spectrum of the THIA in the DCM soaking solution is shown. After about six hours of soaking, in this case, the shape of the absorption band starts changing significantly, which warrants using samples that are soaked for shorter times than that. (d) An increase in absorbance at 424 nm and emission intensity (obtained from integrating the fluorescence spectra) with the time of soaking. It shows saturation after about 15 hours, corresponding to 14 ± 3 μM of THIA in PDMS (see ESI†).

The doping of PDMS relies on the mass transport of the dye from the swelling solution into the thermoset elastomer. As the DCM solvent permeates in the PDMS blocks and swells them (increasing and filling up the volume of the void space between the crosslinked polymer chains), it carries some of the dye molecules into the polymer network. Nevertheless, adsorption of the dye to the stationary polymer chains retards its transport. That is, the dye partitions between DCM and the PDMS, and enhancing its affinity for the latter impedes not only its transport during the initial permeation of the solvent into the blocks but also the diffusion within the swollen polymer network. This partition depends on the nature of the dye and accounts for the drastic differences observed for doping PDMS with Ph-ANI and CR (Fig. 1(h)).

How does PDMS affect the photophysics of THIA and ThT?

Using optical spectroscopy, we characterize the photophysics of THIA and ThT in PDMS and compare them with the results not only for another solid solvent, SOA, but also for non-viscous aprotic liquid solvents with different polarity, *i.e.*, ethyl acetate (EtAc), DCM and *N*,*N*-dimethylformamide (DMF) serve as a comparison (Fig. 3(a) and (b)).

The most critical impact of the rigidity of the solvating media lies on the fluorescence quantum yields, ϕ_f, of THIA and ThT and on the lifetimes (τ) of their emissive excited states. Transferring from liquid to solid solvating media induces a drastic increase in τ of THIA and ThT that amounts to a 400-to-1000 fold (Fig. 4 and Table 1). The fluorescence quantum yields of the two dyes follow the trends of τ (Table 1), resulting in minimal variations of their radiative-decay rate constant, k_f, for the media with different viscosity and polarity (Table 1). Nevertheless, solid solvating media drastically decrease the rate constants of non-radiative deactivation, k_{nd}, consistent with suppressing the conformational degrees of freedom of the dye molecule and preventing the formation of structures leading to the conical intersections between the excited- and ground-state potential-energy surfaces.

Both THIA and ThT are cationic dyes with conformational flexibility that drastically affects their photophysics. Nevertheless, differences in their structural symmetry result in different excited-state dynamics.

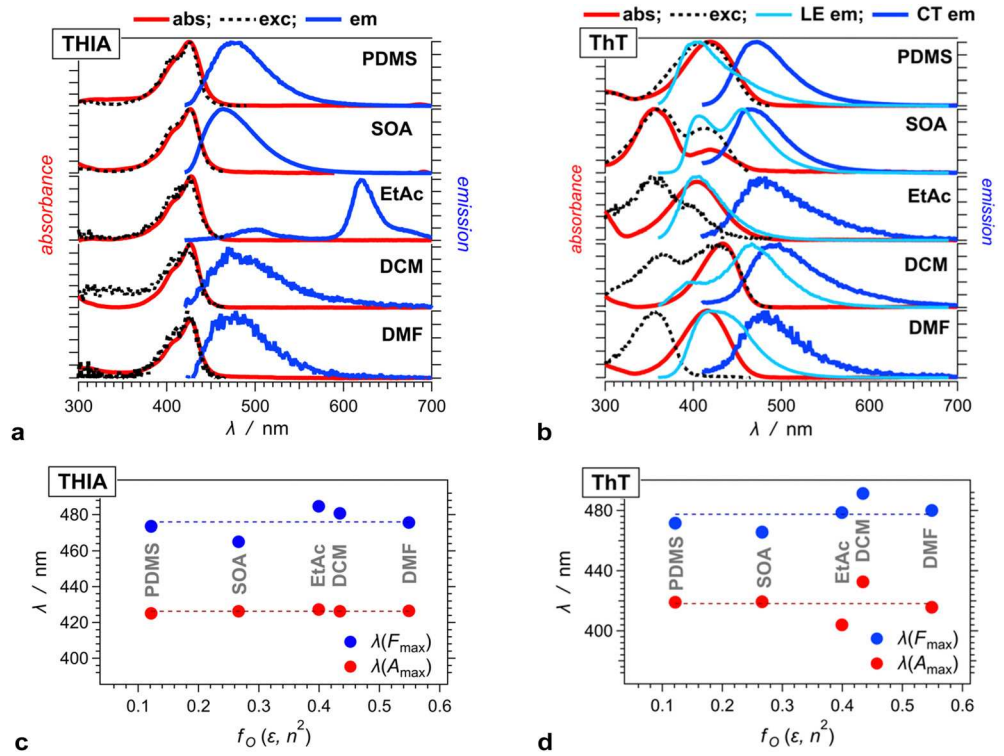

Fig. 3 Solvent dependence of the optical absorption and emission properties of THIA and ThT in different solvents. (a and b) Steady-state absorption (abs), emission (em), and excitation (exc) spectra. For the fluorescence spectra: (a) λ_{ex} = 410 nm, and (b) λ_{ex} = 400 nm for CT em and λ_{ex} = 350 nm for LE em (in the case of the latter, the LE emission is mixed with fluorescence from the CT states); for the excitation spectra (a) λ_{em} = 500 nm for PDMS, and λ_{em} = 470 nm for SOA, EtAc, DCM and DMF; and (b) λ_{em} = 500 nm for PDMS and EtAc, λ_{em} = 500 nm for PDMS, EtAc and DCM, and λ_{em} = 470 nm for SOA and DMF. (c and d) Dependence of the wavelengths of the absorption and fluorescence spectral maxima, $\lambda(A_{max})$ and $\lambda(F_{max})$, respectively, on the Onsager polarity of the solvating medium, $f_O(\varepsilon, n^2) = f_O(\varepsilon) - f_O(n^2)$, where $f_O(x) = 2(x-1)/(2x+1)$[−1,98,99] ε is the medium static dielectric constant: ε_{PDMS} = 2.66,[100] ε_{SOA} = 4.5, ε_{EtAc} = 6.02, ε_{DCM} = 8.93, ε_{DMF} = 36.7, and n^2 is the optical (or dynamic) dielectric constant estimated from the refractive index, n, of the media: n_{PDMS} = 1.42,[101] n_{SOA} = 1.466, n_{EtAc} = 1.3724, n_{DCM} = 1.4241, n_{DMF} = 1.4304. (d) Emission maxima from the spectra recorded with excitation at 400 nm.

THIA: a symmetric cyanine dye. Medium polarity and viscosity have a negligible effect on the THIA absorption, showing spectral maxima at around 425 nm not only for PDMS and SOA but also for the non-viscous aprotic solvents (Fig. 3(a)). For PDMS and DMF, the THIA fluorescence maxima are around 475 nm, and for the other solvents, they range from 465 to 485 nm (Fig. 3(a)). The lack of solvatochromism is consistent with the symmetric structure of the dye and is similar to what we observe for protic solvents with different polarities.[104] The absorption spectra of THIA in alcohols with different polarity and in water show maxima around 425 nm, too, and the produced fluorescence is in the same wavelength range as that for the aprotic solvents we study here.[7,104,105] This trend is consistent with THIA lacking hydrogen-bond accepting groups, which precludes any effects on its photophysics upon transitioning from aprotic to protic solvent environment.

Considering the orientation of the sulphurs and the nitrogens of the two benzothiazolium rings, THIA forms three planar conformers that are fluorescent.[104] In the excited state, rotation of these rings around the bonds that connect them allows THIA to assume twisted conformers that undergo efficient non-radiative deactivation to the ground state.[104] Placing this cyanine dye in viscous media suppresses the ring rotation and the transformation to the twisted conformers. As a result, the non-radiative decay rates decrease substantially and become comparable to the radiative ones, thus, dramatically enhancing the fluorescence quantum yield of THIA.[104] Solid solvating media like PDMS and SOA have the same effect on the photophysics of THIA (Table 1) consistent with limiting its conformational degrees of freedom.

Lowering solvent polarity leads to aggregate formation, as the emergence of an emission band at 620 nm for EtAc reveals (Fig. 3(a)).[106] This spectral feature of THIA aggregation does not appear in the solid solvents despite their low polarity. Because of the suppressed orientational polarization, solid media have inherently lower polarity than liquid solvents.[107,108] That is, while SOA glass and PDMS are less polar than any of the organic solvents we use for this study (Fig. 3(c)), THIA does not show a long-wavelength emission band when dispersed at μM concentrations in either of the two solid media (Fig. 3(a)). The dye is introduced in SOA at elevated temperatures and in PDMS *via* soaking in a DCM solution. Either of these conditions can prevent the formation of the types of ground-state aggregates responsible for the 620-nm emission. Furthermore, the solid media precludes excited-state aggregation and formation of excimers.

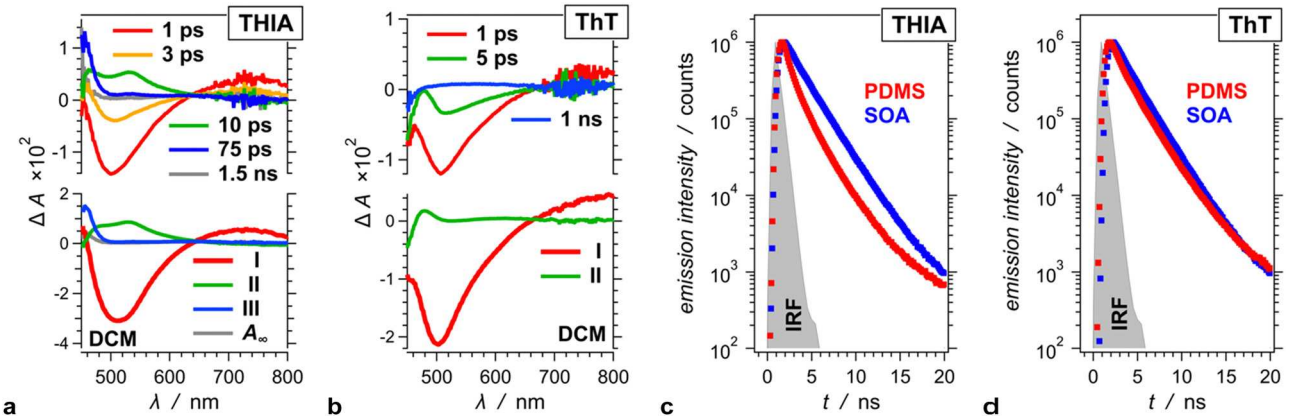

Fig. 4 Time-resolved-spectroscopy analysis of (a) and (c) THIA and (b) and (d) ThT. (a) and (b) For the dyes in non-viscous liquid solvents the picosecond lifetimes of their fluorescence excited states are extracted from pump–probe transient-absorption (TA) analysis (λ_{ex} = 400 nm, instrument-response function (IRF) yields full-width half maximum, FWHM = 200 fs). (c) and (d) For the dyes in solid solvating media, the nanosecond lifetimes of their singlet excites are obtained from fluorescence decays recorded using time-correlated single-photon counting (TCSPC) (λ_{ex} = 406 nm, IRF FWHM = 200 ps).[102] (a) and (b) TA spectra of the two dyes in DCM recorded at different times (upper graphs) and the corresponding evolution-associated differential spectra (EADS) from global-fit analysis (lower graphs). The lifetimes of the fluorescent singlet excited states of the two dyes are extracted from the decay of EADS I (red lines) since they show pronounced stimulated-emission (SE) signals. The global fits of the TA data yield the flowing time constants: (a) τ(I → II) = 2.7 ps, τ(II → III) = 28 ps, and τ(III → A_∞) = 240 ps; and (b) τ(I → II) = 3.4 ps and τ(II → S_0) = 29 ps. (c) and (d) Emission decays of the two dyes in SOA and PDMS recorded at the emission maxima using TCSPC. Multiexponential fits, $F(t) = \Sigma_i \alpha_i \exp(-t\,\tau_i^{-1})$, are implemented in deconvoltuion of the decays with the IRF, and yield: (c) for THIA in PDMS: τ_1 = 0.579 ns (α_1 = 0.78), τ_2 = 1.51 ns (α_2 = 0.19), τ_3 = 2.94 ns (α_3 = 0.03); and for THIA in SOA: τ_1 = 1.05 ns (α_1 = 0.30), τ_2 = 2.38 ns (α_2 = 0.70); (b) for ThT in PDMS: τ_1 = 0.836 ns (α_1 = 0.62), τ_2 = 2.30 ns (α_2 = 0.38); and for ThT in SOA: τ_1 = 0.826 ns (α_1 = 0.30), τ_2 = 2.32 ns (α_2 = 0.70).

Table 1 Photophysical properties of THIA and ThT in different solvation media

	THIA				ThT			
Solvent	$\phi_f{}^a \times 10^{-2}$	τ^b/ps	$k_f{}^c \times 10^{-8}/s^{-1}$	$k_{nd}{}^d \times 10^{-8}/s^{-1}$	$\phi_f{}^a \times 10^{-2}$	τ^b/ps	$k_f{}^c \times 10^{-8}/s^{-1}$	$k_{nd}{}^d \times 10^{-8}/s^{-1}$
EtAc	0.058	2.59	2.2	3900	0.16	2.82	5.7	3000
DCM	0.053	2.73	1.9	3700	0.19	3.35	5.2	2400
DMF	0.070	3.64	1.9	2700	0.17	1.68	10	4900
SOA	43	2190	2.0	2.6	54	2170	2.5	2.1
PDMS	20	1170	1.7	6.8	41	1760	2.3	3.4

[a] Fluorescence quantum yields are obtained from steady-state absorption and emission spectra,[103] λ_{ex} = 410 nm for THIA and λ_{ex} = 400 nm for ThT. [b] Excited-state lifetimes are obtained: (1) for liquid samples, from TA global fits, λ_{ex} = 400 nm (Fig. 4(a) and (b)); and (2) for solid samples, from TCSPC decays, λ_{ex} = 406 nm (Fig. 4(c) and (d)). In the cases of multiexponential decays, intensity-average lifetimes are reported, *i.e.*, $\tau = (\Sigma_i \alpha_i \tau_i^2)(\Sigma_i \alpha_i \tau_i)^{-1}$. [c] Radiative-decay rate constant, $k_f = \phi_f \tau^{-1}$. [d] Nonradiative-decay rate constant, $k_{nd} = (1 - \phi_f)\tau^{-1}$. Indeed, for weakly fluorescent samples, *i.e.*, when $\phi_f \lesssim 10^{-3}$, $k_{nd} \approx \tau^{-1}$.

Although we do not observe the 620-nm emission band of THIA in PDMS, soaking the elastomer for an extended period in DCM solutions with elevated concentrations can perturb the shape of the absorption spectrum of the dye (Fig. 2). Upon extensive soaking of the PDMS, the relative amplitude of the 400-nm shoulder in the absorption band of THIA increases (Fig. 2). This spectral perturbation is consistent with a PDMS-templated formation of H-type ground-state aggregates. Except for the inner-filtering effect at high optical density, however, no changes in the fluorescence spectra of THIA accompany the PDMS-induced alterations of its absorption spectrum. This observation agrees with the inherent lack of fluorescence from H-aggregates.[109] The optical transition from S_0 to the lowest excited state of H-aggregates is forbidden.[109] It results in the observed hypsochromic shifts of the absorption bands originating from transitions to the upper excited states only. Similarly, the radiative deactivation of the lowest excited state of H-aggregates is also forbidden.[109] Thus, the observed THIA fluorescence originates solely from the non-aggregated dye. These considerations preclude the assignment of the 620-nm emission band to fluorescence from an H-aggregate.[106,110–112] Concurrently, formation of such H-type aggregates can lead to an underestimation of the values of ϕ_f and k_f for PDMS. Overall, the 620-nm emission for non-polar liquid solvents originates from aggregates that are different from those that cause the perturbation of the absorption of THIA in PDMS.

ThT: an asymmetric charge-transfer dye. Unlike THIA, ThT is an asymmetric chromophore comprising positively charged 3,6-dimethylbenzothiazolium and electron-rich 4-dimethylaminophenyl (Chart 1) that can act as an electron acceptor and donor, respectively (Scheme 1(a)). Therefore, ThT forms excited states with a charge-transfer (CT) character

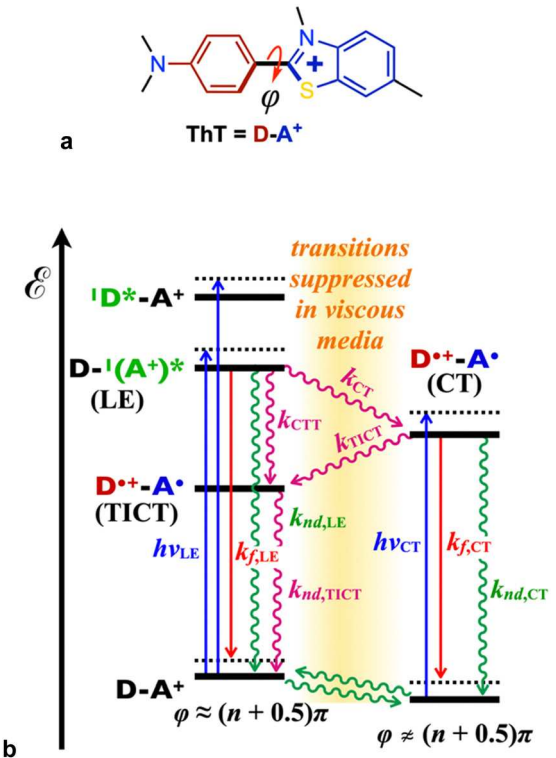

Scheme 1 Ground- and excited-state CT and conformational dynamics of ThT. (a) Electron donor–acceptor (D–A) representation of the ThT cationic structure. The dihedral angle φ between the ring planes of the donor and the acceptor is the key for the dye photophysics.[116] (b) Jablonski diagram showing the ThT photophysics. $\varphi \approx (n + \frac{1}{2})\pi$ represents all structures with orthogonal donor–acceptor geometries (n is an integer). $\varphi \neq (n + \frac{1}{2})\pi$ represents all structures with non-orthogonal donor–acceptor geometries (n is an integer number). The dotted lines correspond to the Franck–Condon states formed after each of the optical vertical transitions: $h\nu$ represents absorption, and k_f – fluorescence. In addition, k_{nd} represents non-radiative decays involving sequential steps of internal conversion and vibrational relaxation; k_{CT} – intramolecular CT involving hole shift from the acceptor to the donor and ring rotation; k_{CTT} – intramolecular CT in the twisted state involving hole shift from the acceptor to the donor without ring rotation; k_{TICT} – formation of a TICT state involving ring rotation and enhancement the extent of the hole shift from the acceptor to the donor.

(Scheme 1(b)).[113–115] Nevertheless, ThT does not display sovatochromism, *i.e.*, neither its absorption nor its fluorescence maxima correlate with the solvent polarity (Fig. 3(b) and (d)). This lack of solvatochromism extends to protic media, such as alcohols with different polarity and water,[6,114] which concurs with the inability of ThT to form hydrogen bonds.

Rather than undergoing charge separation (CS) and generating a CT state with an increased dipole, the photoexcitation of ThT drives a charge shift (CSh) from the cationic acceptor to the electroneutral donor.[117] It warrants considering several factors that can affect the dependence of the optical transitions on the medium polarity: (1) the extent of increasing or decreasing the dipole magnitude of the charged dye upon CSh, which multipole expansions can reveal;[118] (2) the differences between the delocalization of the positive charge when it is on the donor in the CT state and on the acceptor in the locally excited (LE) state;[119] (3) the location and the mobility of the negatively charged counterion; and (4) the dynamic interchange between multiple conformers with different absorption and emission properties. The last is especially important when considering medium viscosity and a dye like ThT with dihedral degrees of freedom that is prone to forming twisted intramolecular charge-transfer (TICT) states (Scheme 1).[3]

The Born solvation energy depends inversely on the ionic radii.[120] Hence, enhancing the localization of the positive charge on the donor upon CSh induces negative solvatochromism.[119] A lack of electrostatic interactions between ThT molecules and the counterions (when they are dispersed in the solution and well separated from one another) is a key assumption for such a purely CSh effect. In solvents that mediate ion pairing, the negatively charged counterion affects the CSh dynamics and the energy of the formed CT state. When the counterion is mobile in non-viscous media, ion transport is accompanied by the shift of the positive charge from the acceptor to the donor. If such ion-transport-coupled CSh increases the dipole of the ion pair, it causes positive solvatochromism. If it reduces the ion-pair dipole, the solvatochromism is negative. When the counterions form ion pairs with ThT in a viscous medium, the intramolecular CSh can lead to CS.[117] The counterion in such ion pairs is most likely immobilized next to the cationic acceptor. CSh moves the positive charge to the donor, away from the negatively charged counterion, and causes CS. It enhances the overall ion-pair dipole and induces positive solvatochromism. These different opposing solvent effects contribute to the lack of distinct dependence of the absorption and fluorescence maxima on the polarity and the viscosity of the media (Fig. 3(d)). In addition, ThT is a molecular rotor (Scheme 1(a)) and can assume multiple conformers with different absorption and emission.[116]

In contrast to THIA, ThT shows drastic differences between its absorption and excitation spectra (Fig. 3(a) and (b)). For the liquid solutions, a 360-nm band emerges in the ThT excitation spectra that do not match any feature in the absorption (Fig. 3(b)). Excitation at 350 nm (where no absorption band is observed) leads to the emergence of a short-wavelength fluorescence band at around 400 nm (Fig. 3(b)). These findings are consistent with small amounts of species (undiscernible on the absorption spectra) that have considerably higher ϕ_f than the abundant form of ThT absorbing at around 420 nm.

For SOA, the absorption and the excitation spectra of ThT show the two peaks at 420 and 360 nm (Fig. 3(b)), suggesting a sufficient abundance of the short-wavelength absorbing species in the solid glass. Excitation at the long-wavelength absorption produces a single-band fluorescence that is quite similar to the ThT emission for the other solvents (Fig. 3(b)). Exciting the short-wavelength band at 350 nm, however, shows dual fluorescence with emission bands at 407 and 455 nm (Fig. 3(b)). Such dual-fluorescence behaviour is not uncommon for dyes comprising directly linked donors and cationic acceptors when dispersed in SOA. Donor-acridinium conjugates in SOA show

450-nm fluorescence from the LE state of the acridinium along with a broad CT emission band in the red spectral region.[36] The solid solvating medium inhibits conformational transformations that mediate the CT step, hence, allowing the emission from the upper, *i.e.*, LE, state to accompany that from the lower, *i.e.*, CT, state. In addition to medium viscosity, solvent polarity can also strongly affect such conformationally driven anti-Kasha behaviour.[40] Moderate donor–acceptor electronic coupling in multicomponent dyes offers an alternative means for attaining broad fluorescence spectra comprising emissions from CT and LE states.[121]

Some reports ascribe the UV band around 350 nm that appears in the absorption spectra of ThT in viscous media, such as glycerol, to impurities or dye aggregates.[114] Considering that the observed hypsochromic absorption originates from H-aggregates precludes a strong fluorescence signal. Radiative deactivation of the lowest states of H-aggregates is not allowed due to the opposing orientation of the transition dipole moments.[109] While we cannot preclude the presence of impurities (especially for the SOA samples that require heating to about 100 °C for their preparation), computational studies provide an alternative explanation about the origin of this UV band.[116] As a molecular rotor, ThT can form multiple conformers with different dihedral angles of the biaryl linker. Small energy barriers separate these rotamers and slow the interexchange between them.[116]

Structures with increased orthogonality between the aromatic rings of the electron donor and acceptor of ThT localize the vertical transitions on the benzothiazolium, resulting in an optical absorption around 360 nm ($h\nu_{LE}$, Scheme 1(b)).[116] Gaining planarity between the donor and acceptor rings: (1) stabilizes the ThT ground state and (2) accommodates overlap between the natural transition orbitals (NTOs) delocalized over the donor and the acceptor. The latter allows a direct optical transition to the CT state ($h\nu_{CT}$, Scheme 1(b)) that dominates the absorption spectra of ThT (Fig. 3(b)).

In non-viscous media, the CT excited state efficiently transitions to a TICT state (k_{TICT}, Scheme 1(b)). The TICT state decays non-radiatively ($k_{nd,TICT}$, Scheme 1(b)) since its orthogonal geometry precludes sufficient overlap between the NTOs for radiative deactivation. This transition of the CT state to a dark TICT state results in the large non-radiative decay rate constants, k_{nd} and the minute ϕ_f of ThT in the liquid non-viscous solvents (Table 1).

The transition from the CT to the TICT state requires a conformational change involving ring rotation. Solid solvating media, such as SOA and PDMS, suppress conformational changes and impede the non-radiative deactivation of the CT state through the TICT pathway (Scheme 1(b)). This effect of rigidity of the solvating environment makes k_{nd} comparable to k_f and increases ϕ_f by orders of magnitude (Table 1).

Photoexcitation of the benzothiazolium LE state in a twisted ThT conformer can drive hole transfer (HT) to the aminophenyl, *i.e.*, CSh leading to the CT or the TICT state. A direct transition from the LE to the TICT state (k_{CTT}, Scheme 1(b)) does not require conformational changes. Nevertheless, the weak donor–acceptor electronic coupling in these twisted conformers warrants slow HT, *i.e.*, small k_{CTT}, which makes the LE state strongly fluorescent. Conversely, HT leading to the CT states (k_{CT}, Scheme 1(b)) requires a conformational change. Deviations of the biaryl dihedral angle, φ, from orthogonality improve the donor–acceptor electronic coupling for CSh. Hence, ring rotation and gaining planarity of the LE state improves the rates of intramolecular CT (k_{CT}, Scheme 1). In addition to the biaryl dihedral angle, the location of the negatively charged counterion in the LE and CT states further dictates the excited-state dynamics. Mobile counterions permit CSh coupled with ion transport, as discussed.[122] Suppose the counterion, however, does not move along with the CSh. In this case, the generated CT state has a larger dipole (and higher energy in non-polar media) than the CT states formed when the anion migrates from the vicinity of the acceptor toward the donor, accompanying the HT.[122,123]

Overall, the relative magnitudes of k_{CT}, k_{CTT} and k_{TICT} (Scheme 1(b)), which depend on medium polarity and viscosity, govern the appearance of the ThT fluorescence spectra upon excitation at 350 nm (Fig. 3(b)). In addition to enhancing the donor–acceptor electronic coupling, the ring rotation leading to planarity increases the overlap between the NTOs of the CT state. Gaining sufficient oscillator strength, the CT structure can undergo radiative deactivation prior to complete relaxation.[116] As a result, for the same solvent the CT fluorescence bands obtained upon excitation at 350 nm can be at shorter wavelengths than the CT emission from 400-nm excitation (Fig. 3(b)). The mismatch between the absorption and excitation spectra of ThT is also a reflection of this synergy between conformational dynamics and CT that governs the radiative deactivation (Fig. 3(b)).

Photoexcitation at 400 nm leads to a Franck–Condon (FC) CT excited state with sufficient planarity that requires a small conformational relaxation to the lowest-lying CT state. Thus, fast vibrational relaxation of the FC CT state ensures that the fluorescence from its relaxed CT structure dominates the emission spectra when excitation is at 400 nm. A transition to the TICT state, however, quenches this fluorescence and results in small ϕ_f.

Following excitation at 350 nm, the transition from the LE to the CT state involves substantial ring rotation and can undergo radiative deactivation prior to assuming the relaxed CT geometry. The inertia of the ring rotation, however, slows the transitions to the TICT states from such non-relaxed CT structures. That is, as the rings rotate away from the orthogonal geometry, the rotation has to stop and turn back in order to form a dark TICT state with $\varphi \approx \pi/2$ or continue through the geometry of the relaxed CT state toward another TICT structure with $\varphi \approx 3\pi/2$. Therefore, the CT fluorescence at 350-nm excitation appears stronger than that from 400-nm excitation. For ThT in DMF, for example, the excitation spectrum monitored at 470 nm shows a distinct band corresponding to the LE absorption and only a barely detectable shoulder in the region where the CT states absorb (Fig. 3(b)).

The optical spectra of ThT in solid-state solvating media reveal how the molecular dynamics of this dye affects its photophysics.

In SOA and PDMS, k_{CT} and k_{TICT} are negligibly small, and k_{CTT} characterizes the only pathway to the TICT state (Scheme 1(b)). The absorption spectrum of ThT in SOA shows transitions to the LE and CT state, at 420 and 360 nm, respectively (Fig. 3(b)). Conversely, ThT in PDMS exhibits only a 420-nm absorption band consistent with direct photoexcitation to the CT state (Fig. 3(b)). The methods of sample preparation can account for this difference. For the SOA solid solutions, the dye needs to be dispersed in the molten medium at around 90 °C. Upon solidifying, the SOA matrix traps the ThT ground-state conformational distribution representative of the population at elevated temperatures. Loading the dye in PDMS, on the other hand, proceeds at room temperature and yields a conformational distribution similar to that in the soaking DCM solution. Hence, the absorption spectrum of ThT in PDMS resembles those in liquid solutions (Fig. 3(b)).

The LE and CT absorption bands of ThT overlap. Thus, 350-nm excitation of ThT in SOA produces fluorescence not only from the LE but also from the CT states even though the solid solvent suppresses the LE → CT transition. Similarly, the LE and the CT fluorescence bands are not well separated. Therefore, the 360-nm LE band emerges in the excitation spectra of ThT in SOA when monitoring the CT fluorescence.

For PDMS, the excitation spectrum of ThT (monitored at 500 nm) shows only a slight broadening and shoulder-like extension around 370 nm without a distinct band in that region (Fig. 3(b)). Even if the twisted ground-state structures are present in minute amounts in the PDMS matrix (as they are in the liquid solutions) and photoexcitation produces the ThT LE state, the rigidity of the polymer environment decreases the likelihood of a transition to a fluorescent state with improved planarity. Excitation of ThT in PDMS at 350 nm produces a single fluorescence band ascribed to the LE emission. The 370-nm shoulder in the excitation spectrum when monitored at the CT emission is a manifestation of the overlap between the LE and the CT fluorescence. Unlike in liquid, non-viscous solvents, the strong fluorescence of ThT in PDMS (due to the suppression of TICT) diminishes the contribution from the overlapping LE emission to the excitation spectra recorded for the CT band. Overall, the spectral feature of the dye dispersed in PDMS represents its photophysics where the large conformational changes are suppressed, *i.e.*, k_{CT} and k_{TICT} are negligibly small (Scheme 1(b)). Unlike SOA, the PDMS samples represent the population distributions in a liquid solvent at room temperature.

Among the wide range of thermoset elastomers available,[124–126] PDMS stands out as one of the best choices for this type of application. (1) It is transparent from the UV to the NIR spectral regions. (2) It does not stick to most organic materials, allowing the use of disposable inexpensive moulds made of common plastics. (3) It reversibly swells in a range of organic solvents allowing facile loading of dyes and other chemical species into its matrix. These three advantages of PDMS as solid solvating media are, indeed, indisputable.

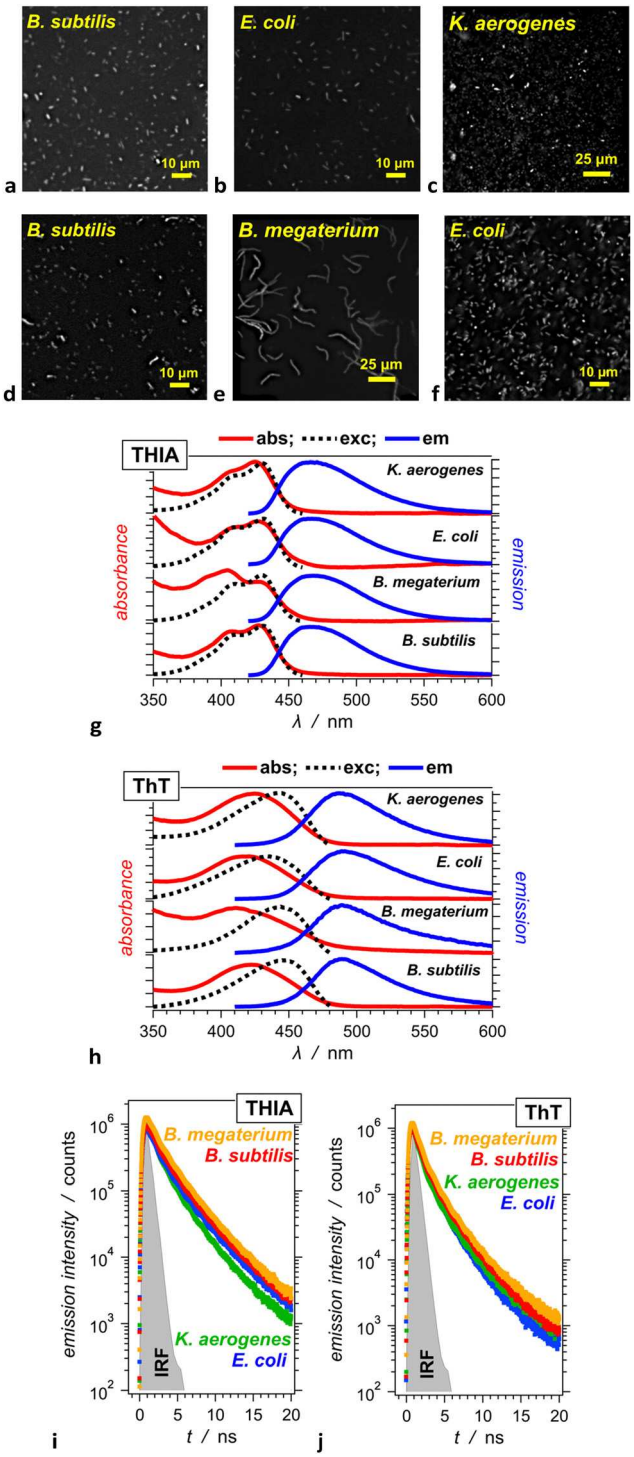

Fig. 5 Staining Gram-positive and Gram-negative bacteria with THIA and ThT in 2 mM Tris buffer, pH 8. Gram-positive species: *Bacillus megaterium* (*B. megaterium*), *Bacillus subtilis* (*B. subtilis*); Gram-negative species: *Escherichia coli* (*E. coli*), *Klebsiella aerogenes* (*K. aerogenes*). *K. aerogenes* is also known as *Enterobacter aerogenes*. (a)–(f) Fluorescence images of bacteria with 10 μM: (a)–(c) THIA and (d)–(f) ThT. (g) and (h) Absorption, emission and excitation spectra, and (i) and (j) TCSPC emission decays of 10 μM (g) and (i) THIA and (h) and (j) ThT in bacterial suspensions (10^7 cell mL^{-1}), λ_{ex} = (g) 410 nm, (h) 400 nm, (i) and (j) 406 nm. Biexponential data fits yield τ_i (α_i): (i) *B. subtilis*: 1.12 ns (0.66), 3.11 ns (0.34); *B. megaterium*: 1.09 ns (0.66), 3.05 ns (0.34); *E. coli*: 1.04 ns (0.70), 3.04 ns (0.30); *K. aerogenes*: 0.953 ns (0.78), 2.71 ns (0.22). (j) *B. subtilis*: 0.735 ns (0.80), 2.38 ns (0.20); *B. megaterium*: 0.775 ns (0.82), 2.46 ns (0.18); *E. coli*: 0.704 ns (0.81), 2.08 ns (0.18); *K. aerogenes*: 0.690 ns (0.87), 2.33 ns (0.13).

Nevertheless, they should not preclude the search for other elastomeric materials that can broaden the application of this methodology. For example, alcohols, water and polar organic solvents do not swell PDMS, which limits the type of dyes and other samples feasible for this technique. Elastomers that show reversible swelling in such solvents can complement the utility of PDMS as a solid medium.

Staining bacterial cells with THIA and ThT

The enormous fluorescence enhancement that medium rigidity can induce on ThT, along with its high propensity for binding to β-strand proteins, has made this dye an indispensable fluorescence probe for imaging amyloid proteins.[4,5] These same properties allow ThT to serve as a photoprobe for fluorescence imaging of bacterial endospores and vegetative prokaryotic cells in biological samples.[6] The abundant β-sheet protein structures in spore coats and in the S-layers of bacterial cell walls allow them to selectively bind ThT and drastically enhance its fluorescence.

Cyanine dyes, such as THIA, have a similar affinity for bacterial cells and have been the foundation for the discovery of dynamic staining.[7,8] Instead of testing if a dye stains the cells or not, the kinetics of fluorescence enhancement (originating from the dye uptake) correlates with the type of the microbial species.[7] It provides opportunities for expanding the staining analytical techniques beyond their binary ''yes/no'' nature.

Adding THIA and ThT solutions to suspensions containing Gram-positive and Gram-negative bacteria allows facile fluorescence imaging of the cells (Fig. 5(a)–(f)). The dye taken up by the prokaryotic cells is strongly fluorescent. Conversely, the unbound dye in the liquid media does not fluoresce and does not interfere with the imaging of the microbial organisms.

It eliminates any need for washing and fixing the cells prior to imaging them, which is one of the greatest advantages of this method of fluorescence staining of prokaryotes. Furthermore, this photolabeling of bacterial spores and vegetative cells does not compromise their vitality and allows for real-time imaging of sporulation and germination, for example.[6]

While τ of THIA and ThT in aqueous media is in the order of a picosecond, mixing THIA and ThT with the bacterial cells increases τ to about 1 to 2 ns (Fig. 5(i) and (j)). These trends of emission enhancement in the biological samples are similar to what we observe when placing these dyes in PDMS solid media (Fig. 4(c) and (d)).

The excitation spectra of ThT bound to Gram-positive and Gram-negative bacterial cells: (1) show only a band with a maximum at around 430–450 nm (Fig. 5(h)), which is similar to the absorption of ThT when bound to amyloid proteins;[114,116] and (2) lack a 360-nm band, which resembles the spectra of ThT in PDMS but not in SOA. The PDMS polymer, therefore, appears to provide a better model of binding such dyes to proteins than the SOA glass does.

Conclusions

The swelling propensity of PDMS in a range of organic solvents provides an attractive means for facile loading of molecular samples under mild conditions. Its optical transparency, along with the ease of its preparation and moulding, make PDMS a promising room-temperature solid-state solvent for a broad range of photophysical applications. In addition to serving as a screening tool for photoprobes that undergo viscosity-induced emission enhancement, PDMS as a solid solvent medium can provide key mechanistic information about excited-state dynamics involving conformational changes. These findings demonstrate the utility of thermoset elastomers as solid solvents in spectroscopy and other photonic applications. While PDMS has some of the most attractive optical and chemical properties for such applications, the search for elastomers that swell in different solvents and can load samples that PDMS cannot significantly broaden the impactful implications of this methodology.

Author contributions

Conceptualization: V. I. V.; methodology: J. A. C., D. B., V. I. V., S. R., L. C. and W. H. G.; software: J. A. C., L. C. and O. O.; validation: J. A. C. and S. R.; formal analysis: J. A. C., S. R., O. O. and V. I. V.; investigation: J. A. C., E. M. E., S. R., D. B., J. B. D. and L. C.; funding acquisition and resources: V. I. V. and W. H. G.; project administration: V. I. V. and J. A. C.; supervision: V. I. V., W. H. G., J. A. C. and O. O.; visualization: J. A. C., L. C. and O. O.; writing – original draft: V. I. V. and J. A. C.; writing – review & editing: V. I. V., J. A. C., S. R., O. O. and W. H. G.

Conflicts of interest

There are no conflicts to declare.

Acknowledgements

The authors thank the U.S.A. National Science Foundation (award CHE 2154609), the U.S.A. National Institutes of Health, National Eye Institute (grant R01 EY027440), and the American Chemical Society Petroleum Research Fund (grant 60651-ND4) for funding this work. W. H. G. and S. R. extend their gratitude to the U.S.A. National Science Foundation (awards DBI 2131428 and CCF 1910878).

Notes and references

1 R. Clark, M. A. Nawawi, A. Dobre, D. Pugh, Q. Liu, A. P. Ivanov, A. J. P. White, J. B. Edel, M. K. Kuimova, A. J. S. McIntosh and T. Welton, The effect of structural heterogeneity upon the microviscosity of ionic liquids, *Chem. Sci.*, 2020, **11**, 6121–6133.
2 N. Amdursky, Y. Erez and D. Huppert, Molecular Rotors: What Lies Behind the High Sensitivity of the Thioflavin-T Fluorescent Marker, *Acc. Chem. Res.*, 2012, **45**, 1548–1557.
3 V. I. Stsiapura, A. A. Maskevich, V. A. Kuzmitsky, V. N. Uversky, I. M. Kuznetsova and K. K. Turoverov, Thioflavin T as a Molecular Rotor: Fluorescent Properties of

Thioflavin T in Solvents with Different Viscosity, *J. Phys. Chem. B*, 2008, **112**, 15893–15902.
4 M. Biancalana and S. Koide, Molecular mechanism of Thioflavin-T binding to amyloid fibrils, *Biochim. Biophys. Acta, Proteins Proteomics*, 2010, **1804**, 1405–1412.
5 N. A. Murugan, J. M. H. Olsen, J. Kongsted, Z. Rinkevicius, K. Aidas and H. Ågren, Amyloid Fibril-Induced Structural and Spectral Modifications in the Thioflavin-T Optical Probe, *J. Phys. Chem. Lett.*, 2013, **4**, 70–77.
6 B. Xia, S. Upadhyayula, V. Nuñez, P. Landsman, S. Lam, H. Malik, S. Gupta, M. Sarshar, J. Hu, B. Anvari, G. Jones and V. I. Vullev, Amyloid histology stain for rapid bacterial endospore imaging, *J. Clin. Microbiol.*, 2011, **49**, 2966–2975.
7 M. S. Thomas, V. Nuñez, S. Upadhyayula, E. R. Zielins, D. Bao, J. M. Vasquez, B. Bahmani and V. I. Vullev, Kinetics of Bacterial Fluorescence Staining with 3,3'-Diethylthiacyanine, *Langmuir*, 2010, **26**, 9756–9765.
8 V. I. Vullev, D. Bao, M. S. Thomas and E. R. Zielins, *Species detection methods and systems*, *US Pat.*, 8252522B2, 2012.
9 J. V. Beitz and J. R. Miller, Exothermic Rate Restrictions on Electron-Transfer in a Rigid Medium, *J. Chem. Phys.*, 1979, **71**, 4579–4595.
10 J. R. Miller, J. V. Beitz and R. K. Huddleston, Effect of Free-Energy on Rates of Electron-Transfer between Molecules, *J. Am. Chem. Soc.*, 1984, **106**, 5057–5068.
11 J. R. Miller, L. T. Calcaterra and G. L. Closs, Intramolecular Long-Distance Electron-Transfer in Radical-Anions - the Effects of Free-Energy and Solvent on the Reaction-Rates, *J. Am. Chem. Soc.*, 1984, **106**, 3047–3049.
12 G. U. Bublitz and S. G. Boxer, Stark spectroscopy: applications in chemistry, biology, and materials science, *Annu. Rev. Phys. Chem.*, 1997, **48**, 213–242.
13 L. Karki, F. W. Vance, J. T. Hupp, S. M. LeCours and M. J. Therien, Electronic stark effect studies of a porphyrin-based push-pull chromophore displaying a large first hyperpolarizability: State-specific contributions to beta, *J. Am. Chem. Soc.*, 1998, **120**, 2606–2611.
14 A. Chowdhury, S. A. Locknar, L. L. Premvardhan and L. A. Peteanu, Effects of Matrix Temperature and Rigidity on the Electronic Properties of Solvatochromic Molecules: Electroabsorption of Coumarin 153, *J. Phys. Chem. A*, 1999, **103**, 9614–9625.
15 H. T. Shi, Z. Cai, J. Patrow, B. F. Zhao, Y. Wang, Y. Wang, A. Benderskii, J. Dawlaty and S. B. Cronin, Monitoring Local Electric Fields at Electrode Surfaces Using Surface Enhanced Raman Scattering-Based Stark-Shift Spectroscopy during Hydrogen Evolution Reactions, *ACS Appl. Mater. Interfaces*, 2018, **10**, 33678–33683.
16 G. B. Strambini, Fluorescence and phosphorescence methods to probe protein structure and stability in ice: the case of azurin, in *Formulation and Process Development Strategies for Manufacturing Biopharmaceuticals*, John Wiley & Sons, Inc., 2010, pp. 207–229.
17 W. B. Wilson, E. C. Heider, A. D. Campiglia and F. Barbosa, Jr., Low-temperature multidimensional luminescence spectroscopy for the analysis of polycyclic aromatic compounds, *Curr. Top. Anal. Chem.*, 2012, **9**, 1–23.
18 O. S. Wenger, Photoinduced electron tunneling between randomly dispersed donors and acceptors in frozen glasses and other rigid matrices, *Phys. Chem. Chem. Phys.*, 2013, **15**, 10673–10685.
19 I. S. Osad'ko and E. V. Khots, Scan time dependence of single molecule optical lines in polymers and glasses, *Single Mol.*, 2002, **3**, 236–246.
20 W. Huang, Zeolites as host matrix for luminescent carbon dots: a new class of thermally activated delayed fluorescence materials with 350 ms delayed decay time, *Sci. China: Chem.*, 2017, **60**, 1147–1148.
21 K. Shizu, J. Lee, H. Tanaka, H. Nomura, T. Yasuda, H. Kaji and C. Adachi, Highly efficient electroluminescence from purely organic donor-acceptor systems, *Pure Appl. Chem.*, 2015, **87**, 627–638.
22 S. Kowalak, A. Jankowska and A. Zywert, Pigments with molecular sieve matrices, *Curr. Phys. Chem.*, 2012, **2**, 200–210.
23 J. Moreda-Pineiro, E. Alonso-Rodriguez, P. Lopez-Mahia, S. Muniategui-Lorenzo, D. Prada-Rodriguez, P. Lopez-Mahia, D. Prada-Rodriguez, V. Romaris-Hortas, M. Miguez-Framil, A. Moreda-Pineiro and P. Bermejo-Barrera, Matrix solid-phase dispersion of organic compounds and its feasibility for extracting inorganic and organometallic compounds, *TrAC, Trends Anal. Chem.*, 2008, **28**, 110–116.
24 G. Calzaferri and K. Lutkouskaya, Mimicking the antenna system of green plants, *Photochem. Photobiol. Sci.*, 2008, **7**, 879–910.
25 G. Calzaferri, H. Li and D. Bruhwiler, Dye-modified nanochannel materials for photoelectronic and optical devices, *Chem. – Eur. J.*, 2008, **14**, 7442–7449.
26 M. B. J. Roeffaers, J. Hofkens, G. De Cremer, F. C. De Schryver, P. A. Jacobs, D. E. De Vos and B. F. Sels, Fluorescence microscopy: Bridging the phase gap in catalysis, *Catal. Today*, 2007, **126**, 44–53.
27 D. Bizzotto and J. L. Shepherd, Epi-fluorescence microscopy studies of potential controlled changes in adsorbed thin organic films at electrode surfaces, *Adv. Electrochem. Sci. Eng.*, 2006, **9**, 97–126.
28 V. Ramamurthy, Weak interactions between organic molecules and alkali metal ions present in zeolites help manipulate the excited state behavior of organic molecules, *J. Photosci.*, 2003, **10**, 127–148.
29 I. Ichinose and T. Kunitake, Wrapping and inclusion of organic molecules with ultrathin, amorphous metal oxide films, *Chem. Rec.*, 2002, **2**, 339–351.
30 G. Calzaferri, Organic-inorganic composites as photonic antenna, *Chimia*, 2001, **55**, 1009–1013.
31 V. Talbot and M. Bianchi, Use of fluorogenic model substrates for extracellular bacterial enzyme activity (EEA), *Oceanis*, 1995, **21**, 247.
32 S. Hashimoto, Zeolite photochemistry: impact of zeolites on photochemistry and feedback from photochemistry to zeolite science, *J. Photochem. Photobiol., C*, 2003, **4**, 19–49.

33 R. P. Domingue and M. D. Fayer, Electron transfer between molecules randomly distributed in a glass, *J. Chem. Phys.*, 1985, **83**, 2242.
34 L. Song, S. F. Swallen, R. C. Dorfman, K. Weidemaier and M. D. Fayer, Photoinduced Electron-Transfer and Geminate Recombination in Solution, *J. Phys. Chem.*, 1993, **97**, 1374–1382.
35 C. Burgdorff and H. G. Loehmannsroeben, Photophysical properties of tetracene derivatives in solution. III. Thermally activated nonradiative processes and triplet state properties, *J. Lumin.*, 1994, **59**, 201–208.
36 G. Jones, II, D. Yan, J. Hu, J. Wan, B. Xia and V. I. Vullev, Photoinduced Electron Transfer in Arylacridinium Conjugates in a Solid Glass Matrix, *J. Phys. Chem. B*, 2007, **111**, 6921–6929.
37 H. Sato, V. Kathirvelu, A. Fielding, J. P. Blinco, A. S. Micallef, S. E. Bottle, S. S. Eaton and G. R. Eaton, Impact of molecular size on electron spin relaxation rates of nitroxyl radicals in glassy solvents between 100 and 300 K, *Mol. Phys.*, 2007, **105**, 2137–2151.
38 Y. M. Poronik, G. V. Baryshnikov, I. Deperasinska, E. M. Espinoza, J. A. Clark, H. Agren, D. T. Gryko and V. I. Vullev, Deciphering the unusual fluorescence in weakly coupled bis-nitro-pyrrolo[3,2-b]pyrroles, *Commun. Chem.*, 2020, **3**, 190.
39 B. Sadowski, M. Kaliszewska, Y. M. Poronik, M. Czichy, P. Janasik, M. Banasiewicz, D. Mierzwa, W. Gadomski, T. D. Lohrey, J. A. Clark, M. Lapkowski, B. Kozankiewicz, V. I. Vullev, A. L. Sobolewski, P. Piatkowski and D. T. Gryko, Potent strategy towards strongly emissive nitroaromatics through a weakly electron-deficient core, *Chem. Sci.*, 2021, **12**, 14039–14049.
40 K. Szychta, B. Koszarna, M. Banasiewicz, A. Sobolewski, O. Omari, J. A. Clark, V. I. Vullev, C. A. Barboza and D. T. Gryko, Conformation of the Ester Group Governs the Photophysics of Highly Polarized Benzo[g]coumarins, *JACS Au*, 2023, **3**, 1918–1930.
41 C. H. Jiang, M. G. Kuzyk, J. L. Ding, W. E. Johns and D. J. Welker, Fabrication and mechanical behavior of dye-doped polymer optical fiber, *J. Appl. Phys.*, 2002, **92**, 4–12.
42 L. F. Paz, M. Caño-García, M. A. Geday, J. M. Otón and X. Quintana, Identification of dyes and matrices for dye doped polymer waveguide emitters covering the visible spectrum, *Sci. Rep.*, 2022, **12**, 6142.
43 A. U. Acuña, F. Amat-Guerri, A. Costela, A. Douhal, J. M. Figuera, F. Florido and R. Sastre, Proton-transfer lasing from solid organic matrices, *Chem. Phys. Lett.*, 1991, **187**, 98–102.
44 K. M. Dyumaev, A. A. Manenkov, A. P. Maslyukov, G. A. Matyushin, V. S. Nechitailo and A. M. Prokhorov, Dyes in modified polymers:, problems of photostability and conversion efficiency at high intensities, *J. Opt. Soc. Am. B*, 1992, **9**, 143–151.
45 F. Amat-Guerri, A. Costela, J. M. Figuera, F. Florido and R. Sastre, Laser action from rhodamine 6G-doped poly (2-hydroxyethyl methacrylate) matrices with different cross-linking degrees, *Chem. Phys. Lett.*, 1993, **209**, 352–356.
46 C. Fleischmann, M. Lievenbrück and H. Ritter, Polymers and Dyes: Developments and Applications, *Polymers*, 2015, **7**, 717–746.
47 M. Plouzeau, S. Piogé, F. Peilleron, L. Fontaine and S. Pascual, Polymer/dye blends: Preparation and optical performance: A short review, *J. Appl. Polym. Sci.*, 2022, **139**, e52861.
48 O. Hofmann, X. Wang, A. Cornwell, S. Beecher, A. Raja, D. D. C. Bradley, A. J. deMello and J. C. deMello, Monolithically integrated dye-doped PDMS long-pass filters for disposable on-chip fluorescence detection, *Lab Chip*, 2006, **6**, 981–987.
49 R. Xue, P. Behera, J. Xu, M. S. Viapiano and J. J. Lannutti, Polydimethylsiloxane core–polycaprolactone shell nanofibers as biocompatible, real-time oxygen sensors, *Sens. Actuators, B*, 2014, **192**, 697–707.
50 A. Angelini, F. Pirani, F. Frascella and E. Descrovi, Reconfigurable elastomeric graded-index optical elements controlled by light, *Light: Sci. Appl.*, 2018, **7**, 7.
51 A. Angelini, U. Agero, F. Ferrarese Lupi, M. Fretto, F. Pirri and F. Frascella, Real-time and reversible light-actuated microfluidic channel squeezing in dye-doped PDMS, *Soft Matter*, 2020, **16**, 4383–4388.
52 F. Ciardelli, G. Ruggeri and A. Pucci, Dye-containing polymers: methods for preparation of mechanochromic materials, *Chem. Soc. Rev.*, 2013, **42**, 857–870.
53 A. Ishchenko, Molecular engineering of dye-doped polymers for optoelectronics, *Polym. Adv. Technol.*, 2002, **13**, 744–752.
54 K.-S. Chang, Y.-C. Chung, T.-H. Yang, S. J. Lue, K.-L. Tung and Y.-F. Lin, Free volume and alcohol transport properties of PDMS membranes: Insights of nano-structure and interfacial affinity from molecular modeling, *J. Membr. Sci.*, 2012, **417–418**, 119–130.
55 T. C. Merkel, V. I. Bondar, K. Nagai, B. D. Freeman and I. Pinnau, Gas sorption, diffusion, and permeation in poly(dimethylsiloxane), *J. Polym. Sci., Part B: Polym. Phys.*, 2000, **38**, 415–434.
56 N. Petzetakis, C. M. Doherty, A. W. Thornton, X. C. Chen, P. Cotanda, A. J. Hill and N. P. Balsara, Membranes with artificial free-volume for biofuel production, *Nat. Commun.*, 2015, **6**, 7529.
57 M. Sadrzadeh, K. Shahidi and T. Mohammadi, Synthesis and gas permeation properties of a single layer PDMS membrane, *J. Appl. Polym. Sci.*, 2010, **117**, 33–48.
58 M. Adiraj Iyer and D. T. Eddington, Storing and releasing rhodamine as a model hydrophobic compound in polydimethylsiloxane microfluidic devices, *Lab Chip*, 2019, **19**, 574–579.
59 K. Nakakubo, D. Takagoshi, Y. Mikami, H. Yoshioka, T. Kotani and Y. Oki, Solid phase dye molecular dispersion property of PDMS-based thermoplastic elastomer, *Opt. Mater. Express*, 2022, **12**, 196–203.
60 H. Yoshioka, Y. Itoh, A. Kiyomori, M. Era and Y. Oki, Fluorene-based chromophore for degradation-recoverable solid-state dye laser, *Opt. Mater. Express*, 2013, **3**, 176–183.

61 J. A. Rogers, R. J. Jackman, O. J. A. Schueller and G. M. Whitesides, Elastomeric diffraction gratings as photothermal detectors, *Appl. Opt.*, 1996, **35**, 6641–6647.
62 N. Bowden, I. S. Choi, B. A. Grzybowski and G. M. Whitesides, Mesoscale Self-Assembly of Hexagonal Plates Using Lateral Capillary Forces: Synthesis Using the ''Capillary Bond'', *J. Am. Chem. Soc.*, 1999, **121**, 5373–5391.
63 J. Wan, S. Zhou, H. J. Mea, Y. Guo, H. Ku and B. M. Urbina, Emerging Roles of Microfluidics in Brain Research: From Cerebral Fluids Manipulation to Brain-on-a-Chip and Neuroelectronic Devices Engineering, *Chem. Rev.*, 2022, **122**, 7142–7181.
64 M. S. Thomas, B. Millare, J. M. Clift, D. Bao, C. Hong and V. I. Vullev, Print-and-peel fabrication for microfluidics: what's in it for biomedical applications?, *Ann. Biomed. Eng.*, 2010, **38**, 21–32.
65 J. C. McDonald and G. M. Whitesides, Poly(dimethylsiloxane) as a Material for Fabricating Microfluidic Devices, *Acc. Chem. Res.*, 2002, **35**, 491–499.
66 V. I. Vullev, J. Wan, V. Heinrich, P. Landsman, P. E. Bower, B. Xia, B. Millare and G. Jones, II, Nonlithographic Fabrication of Microfluidic Devices, *J. Am. Chem. Soc.*, 2006, **128**, 16062–16072.
67 V. Nuñez, S. Upadhyayula, B. Millare, J. M. Larsen, A. Hadian, S. Shin, P. Vandrangi, S. Gupta, H. Xu, A. P. Lin, G. Y. Georgiev and V. I. Vullev, Microfluidic Space-Domain Time-Resolved Emission Spectroscopy of Terbium(III) and Europium(III) Chelates with Pyridine-2,6-Dicarboxylate, *Anal. Chem.*, 2013, **85**, 4567–4577.
68 J. Liu, M. Enzelberger and S. Quake, A nanoliter rotary device for polymerase chain reaction, *Electrophoresis*, 2002, **23**, 1531–1536.
69 C. Hong, D. Bao, M. S. Thomas, J. M. Clift and V. I. Vullev, Print-and-Peel Fabrication of Microelectrodes, *Langmuir*, 2008, **24**, 8439–8442.
70 M. S. Thomas, J. M. Clift, B. Millare and V. I. Vullev, Print-and-Peel Fabricated Passive Micromixers, *Langmuir*, 2010, **26**, 2951–2957.
71 A. S. Smith, R. B. Nowak, S. T. Zhou, M. Giannetto, D. S. Gokhin, J. Papoin, I. C. Ghiran, L. Blanc, J. D. Wan and V. M. Fowler, Myosin IIA interacts with the spectrin-actin membrane skeleton to control red blood cell membrane curvature and deformability, *Proc. Natl. Acad. Sci. U. S. A.*, 2018, **115**, E6385–E6385.
72 B. T. Mayers, D. V. Vezenov, V. I. Vullev and G. M. Whitesides, Arrays and Cascades of Fluorescent Liquid-Liquid Waveguides: Broadband Light Sources for Spectroscopy in Microchannels, *Anal. Chem.*, 2005, **77**, 1310–1316.
73 J. N. Lee, C. Park and G. M. Whitesides, Solvent Compatibility of Poly(dimethylsiloxane)-Based Microfluidic Devices, *Anal. Chem.*, 2003, **75**, 6544–6554.
74 V. Prajzler, M. Neruda and P. Nekvindová, Flexible multimode polydimethyl-diphenylsiloxane optical planar waveguides, *J. Mater. Sci.: Mater. Electron.*, 2018, **29**, 5878–5884.
75 M. H. Wu, K. E. Paul and G. M. Whitesides, Patterning flood illumination with microlens arrays, *Appl. Opt.*, 2002, **41**, 2575–2585.
76 S.-K. Chae, J.-H. Ryoo and S.-H. Lee, Thin and large free-standing PDMS membrane by using polystyrene Petri dish, *BioChip J.*, 2012, **6**, 184–190.
77 B. Millare, M. Thomas, A. Ferreira, H. Xu, M. Holesinger and V. I. Vullev, Dependence of the quality of adhesion between polydimethyl siloxane and glass surfaces on the conditions of treatment with oxygen plasma, *Langmuir*, 2008, **24**, 13218–13224.
78 K. Chau, B. Millare, A. Lin, S. Upadhyayula, V. Nuñez, H. Xu and V. I. Vullev, Dependence of the quality of adhesion between poly(dimethylsiloxane) and glass surfaces on the composition of the oxidizing plasma, *Microfluid. Nanofluid.*, 2011, **10**, 907–917.
79 Y. L. Wang, J. Balowski, C. Phillips, R. Phillips, C. E. Sims and N. L. Allbritton, Benchtop micromolding of polystyrene by soft lithography, *Lab Chip*, 2011, **11**, 3089–3097.
80 S. Banik, A. Uchil, T. Kalsang, S. Chakrabarty, M. A. Ali, P. Srisungsitthisunti, K. K. Mahato, S. Surdo and N. Mazumder, The revolution of PDMS microfluidics in cellular biology, *Crit. Rev. Biotechnol.*, 2023, **43**, 465–483.
81 D. Torres-Alvarez and A. Aguirre-Soto, Polydimethylsiloxane chemistry for the fabrication of microfluidics-Perspective on its uniqueness, limitations and alternatives, *Mater. Today: Proc.*, 2022, **48**, 88–95.
82 I. Miranda, A. Souza, P. Sousa, J. Ribeiro, E. M. S. Castanheira, R. Lima and G. Minas, Properties and Applications of PDMS for Biomedical Engineering: A Review, *J. Funct. Biomater.*, 2022, **13**, 2.
83 G. M. Whitesides, The origins and the future of microfluidics, *Nature*, 2006, **442**, 368–373.
84 Y. Zeng, J. W. Khor, T. L. van Neel, W.-C. Tu, J. Berthier, S. Thongpang, E. Berthier and A. B. Theberge, Miniaturizing chemistry and biology using droplets in open systems, *Nat. Rev. Chem.*, 2023, **7**, 439–455.
85 J. Panwar, A. Autour and C. A. Merten, Design and construction of a microfluidics workstation for high-throughput multi-wavelength fluorescence and transmittance activated droplet analysis and sorting, *Nat. Protoc.*, 2023, **18**, 1090–1136.
86 F. Paratore, V. Bacheva, M. Bercovici and G. V. Kaigala, Reconfigurable microfluidics, *Nat. Rev. Chem.*, 2022, **6**, 70–80.
87 T. Bhardwaj and T. K. Sharma, Nanosensor-Enabled Microfluidic Biosensors for the Detection of Pathogenic Bacteria, in *Nanosensors for Point-of-Care Diagnostics of Pathogenic Bacteria*, ed. A. Acharya and N. K. Singhal, Springer Nature Singapore, Singapore, 2023, pp. 85–111.
88 Q. Ma and J. Xu, Green microfluidics in microchemical engineering for carbon neutrality, *Chin. J. Chem. Eng.*, 2023, **53**, 332–345.
89 R. Thakur and G. Y. Fridman, Low Cost, Ease-of-Access Fabrication of Microfluidic Devices Using Wet Paper Molds, *Micromachines*, 2022, **13**, 1408.

90 Y. You, M.-J. Kim, G.-N. Ahn, S. Bae, D. Kim, J.-K. Kim, Y. Kwon, J. Ryu, J. Lee and D.-P. Kim, Bimodal Light-Harvesting Microfluidic System Using Upconversion Nanocrystals for Enhanced Flow Photocatalysis, *Adv. Mater. Technol.*, 2022, **7**, 2101656.
91 B. Sharma and A. Sharma, Microfluidics: Recent Advances Toward Lab-on-Chip Applications in Bioanalysis, *Adv. Eng. Mater.*, 2022, **24**, 2100738.
92 G. Gonzalez, I. Roppolo, C. F. Pirri and A. Chiappone, Current and emerging trends in polymeric 3D printed microfluidic devices, *Addit. Manuf.*, 2022, **55**, 102867.
93 E. Jagtiani, M. Yeolekar, S. Naik and V. Patravale, In vitro blood brain barrier models: An overview, *J. Controlled Release*, 2022, **343**, 13–30.
94 T. Bhardwaj, L. N. Ramana and T. K. Sharma, Current Advancements and Future Road Map to Develop ASSURED Microfluidic Biosensors for Infectious and Non-Infectious Diseases, *Biosensors*, 2022, **12**, 357.
95 T. Bardelli, C. Marano and F. Briatico Vangosa, Polydimethylsiloxane crosslinking kinetics: A systematic study on Sylgard184 comparing rheological and thermal approaches, *J. Appl. Polym. Sci.*, 2021, **138**, 51013.
96 D. Bao, B. Millare, W. Xia, B. G. Steyer, A. A. Gerasimenko, A. Ferreira, A. Contreras and V. I. Vullev, Electrochemical Oxidation of Ferrocene: A Strong Dependence on the Concentration of the Supporting Electrolyte for Nonpolar Solvents, *J. Phys. Chem. A*, 2009, **113**, 1259–1267.
97 O. O'Mari and V. I. Vullev, Optical Window to Polarity of Electrolyte Solutions, *Molecules*, 2023, **28**, 4360.
98 M. F. Mayther, O. O'Mari, P. Flacke, D. Bhatt, S. Andrews and V. I. Vullev, How Do Liquid-Junction Potentials and Medium Polarity at Electrode Surfaces Affect Electrochemical Analyses for Charge-Transfer Systems?, *J. Phys. Chem. B*, 2023, **127**, 1443–1458.
99 L. Onsager, Electric moments of molecules in liquids, *J. Am. Chem. Soc.*, 1936, **58**, 1486–1493.
100 P. K. Sharma, N. Gupta and P. I. Dankov, Characterization of polydimethylsiloxane (PDMS) as a wearable antenna substrate using resonance and planar structure methods, *Int. J. Electron. Commun.*, 2020, **127**, 153455.
101 C. Meichner, A. E. Schedl, C. Neuber, K. Kreger, H. W. Schmidt and L. Kador, Refractive-index determination of solids from first- and second-order critical diffraction angles of periodic surface patterns, *AIP Adv.*, 2015, **5**, 087135.
102 H. Lu, D. Bao, M. Penchev, M. Ghazinejad, V. I. Vullev, C. S. Ozkan and M. Ozkan, Pyridine-coated lead sulfide quantum dots for polymer hybrid photovoltaic devices, *Adv. Sci. Lett.*, 2010, **3**, 101–109.
103 G. Jones, II and V. I. Vullev, Medium Effects on the Stability of Terbium(III) Complexes with Pyridine-2,6-dicarboxylate, *J. Phys. Chem. A*, 2002, **106**, 8213–8222.
104 S. Upadhyayula, V. Nunez, E. M. Espinoza, J. M. Larsen, D. Bao, D. Shi, J. T. Mac, B. Anvari and V. I. Vullev, Photoinduced dynamics of a cyanine dye: parallel pathways of non-radiative deactivation involving multiple excited-state twisted transients, *Chem. Sci.*, 2015, **6**, 2237–2251.
105 M. Mohankumar, M. Unnikrishnan, G. N. Naidu, S. M. Somasundaran, M. P. Ajaykumar, R. S. Swathi and K. G. Thomas, Finding the Needle in a Haystack: Capturing Veiled Plexcitonic Coupling through Differential Spectroscopy, *J. Phys. Chem. C*, 2020, **124**, 26387–26395.
106 A. K. Mandal and M. K. Pal, Strong fluorescence emissions by H-aggregates of the dye thiacyanine in the presence of the surfactant aerosol-OT, *Chem. Phys.*, 2000, **253**, 115–124.
107 S. Upadhyayula, D. Bao, B. Millare, S. S. Sylvia, K. M. M. Habib, K. Ashraf, A. Ferreira, S. Bishop, R. Bonderer, S. Baqai, X. Jing, M. Penchev, M. Ozkan, C. S. Ozkan, R. K. Lake and V. I. Vullev, Permanent Electric Dipole Moments of Carboxyamides in Condensed Media: What Are the Limitations of Theory and Experiment?, *J. Phys. Chem. B*, 2011, **115**, 9473–9490.
108 M. R. Brindza and R. A. Walker, Differentiating Solvation Mechanisms at Polar Solid/Liquid Interfaces, *J. Am. Chem. Soc.*, 2009, **131**, 6207–6214.
109 M. Kasha, H. R. Rawls and M. Ashraf El-Bayoumi, The exciton model in molecular spectroscopy, *Pure Appl. Chem.*, 1965, **11**, 371–392.
110 O.-K. Kim, J. Je, G. Jernigan, L. Buckley and D. Whitten, Super-Helix Formation Induced by Cyanine J-Aggregates onto Random-Coil Carboxymethyl Amylose as Template, *J. Am. Chem. Soc.*, 2006, **128**, 510–516.
111 H. Tobata and T. Sagawa, Specific excitonic interactions in the aggregates of hyaluronic acid and cyanine dyes with different lengths of methine group, *Photochem. Photobiol. Sci.*, 2016, **15**, 329–333.
112 A. Kumar Mandal and M. Kanta Pal, Spectral analysis of complexes of the dye, 3,3′-diethyl thiacyanine and the anionic surfactant, SDS by the principal component analysis method, *Spectrochim. Acta, Part A*, 1999, **55**, 1347–1358.
113 A. Islam, Y. Kikuchi and T. Iimori, Electroabsorption and Stark Fluorescence Spectroscopies of Thioflavin T, *J. Phys. Chem. A*, 2023, **127**, 1436–1444.
114 E. S. Voropai, M. P. Samtsov, K. N. Kaplevskii, A. A. Maskevich, V. I. Stepuro, O. I. Povarova, I. M. Kuznetsova, K. K. Turoverov, A. L. Fink and V. N. Uverskii, Spectral Properties of Thioflavin T and Its Complexes with Amyloid Fibrils, *J. Appl. Spectrosc.*, 2003, **70**, 868–874.
115 P. K. Singh, M. Kumbhakar, H. Pal and S. Nath, Viscosity Effect on the Ultrafast Bond Twisting Dynamics in an Amyloid Fibril Sensor: Thioflavin-T, *J. Phys. Chem. B*, 2010, **114**, 5920–5927.
116 A. A. Maskevich, V. I. Stsiapura, V. A. Kuzmitsky, I. M. Kuznetsova, O. I. Povarova, V. N. Uversky and K. K. Turoverov, Spectral Properties of Thioflavin T in Solvents with Different Dielectric Properties and in a Fibril-Incorporated Form, *J. Proteome Res.*, 2007, **6**, 1392–1401.
117 J. B. Derr, J. Tamayo, J. A. Clark, M. Morales, M. F. Mayther, E. M. Espinoza, K. Rybicka-Jasinska and V. I. Vullev,

Multifaceted aspects of charge transfer, *Phys. Chem. Chem. Phys.*, 2020, **22**, 21583–21629.

118 M. Krzeszewski, E. M. Espinoza, C. Cervinka, J. B. Derr, J. A. Clark, D. Borchardt, G. J. O. Beran, D. T. Gryko and V. I. Vullev, Dipole Effects on Electron Transfer are Enormous, *Angew. Chem., Int. Ed.*, 2018, **57**, 12365–12369.

119 J. Hu, B. Xia, D. Bao, A. Ferreira, J. Wan, G. Jones and V. I. Vullev, Long-Lived Photogenerated States of α-Oligothiophene-Acridinium Dyads Have Triplet Character, *J. Phys. Chem. A*, 2009, **113**, 3096–3107.

120 M. Born, Volumes and heats of hydration of ions, *Z. Phys.*, 1920, **1**, 45–48.

121 J. A. Clark, D. Kusy, O. Vakuliuk, M. Krzeszewski, K. J. Kochanowski, B. Koszarna, O. O'Mari, D. Jacquemin, D. T. Gryko and V. I. Vullev, The magic of biaryl linkers: the electronic coupling through them defines the propensity for excited-state symmetry breaking in quadrupolar acceptor–donor–acceptor fluorophores, *Chem. Sci.*, 2023, **14**, 13537–13550.

122 K. Rybicka-Jasińska and V. I. Vullev, *Charge Transfer & Organic Photoelectrochemistry, in ACS in Focus*, American Chemical Society, 2023.

123 J. B. Derr, J. Tamayo, E. M. Espinoza, J. A. Clark and V. I. Vullev, Dipole-induced effects on charge transfer and charge transport. Why do molecular electrets matter?, *Can. J. Chem.*, 2018, **96**, 843–858.

124 J. E. Mark, Thermoset Elastomers, in *Applied Plastics Engineering Handbook*, ed. M. Kutz, William Andrew Publishing, 2nd edn, 2017, pp. 109–125.

125 J. Luo, Z. Demchuk, X. Zhao, T. Saito, M. Tian, A. P. Sokolov and P.-F. Cao, Elastic vitrimers: Beyond thermoplastic and thermoset elastomers, *Matter*, 2022, **5**, 1391–1422.

126 A. R. Webb, J. Yang and G. A. Ameer, A new strategy to characterize the extent of reaction of thermoset elastomers, *J. Polym. Sci., Part A: Polym. Chem.*, 2008, **46**, 1318–1328.

